Supporting Information

High-Entropy FeCoMnCuNi diselenide Self-Standing Electrode with Outstanding Water-Electrolysis Performance in Alkaline Medium

Xinxin Guo [a, †], Mengmeng Zhou [a, †], Ziwu Liu [a, *], Shiheng Mu [a], Kaijia Wang [a], Huanqiang Shi [a], Fang Wang [a, b] **, Zhonghai Ni [a] and Guiqing Liu [b, ***]

[a] Jiangsu Key Laboratory of Coal-based Greenhouse Gas Control and Utilization, School of Chemical Engineering and Jiangsu Province Engineering Laboratory of High Efficient Energy Storage Technology and Equipments, China University of Mining & Technology, Xuzhou 221008, Jiangsu, China

[b] Jiangsu BGRIMM Metal Recycling Science & Technology Co., Ltd, Xuzhou 221008, Jiangsu, China

† These authors contributed equally to this work.

*Corresponding author, Email address: lzwmsy@cumt.edu.cn, Fax: 86-516-83883501.

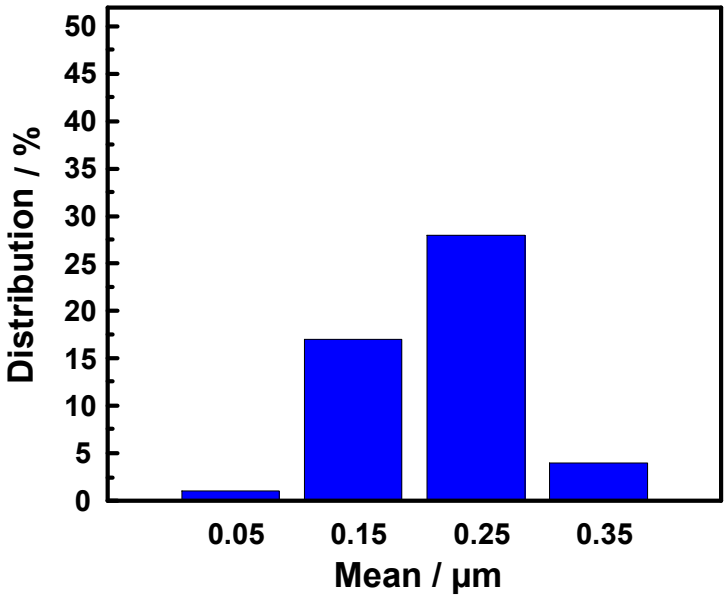

Fig. S1 The thickness-distribution histograms of petunia leaves on the surface of

$FeCoMnCuNiSe_2$.

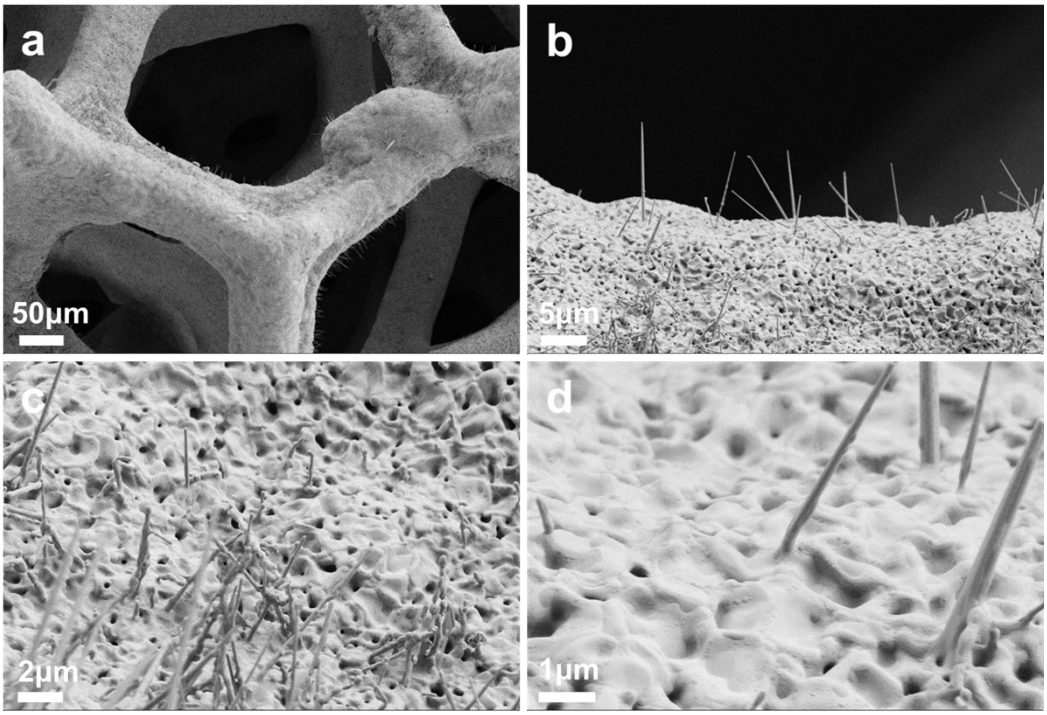

Fig. S2 The SEM images of selenized bare NF (a-d).

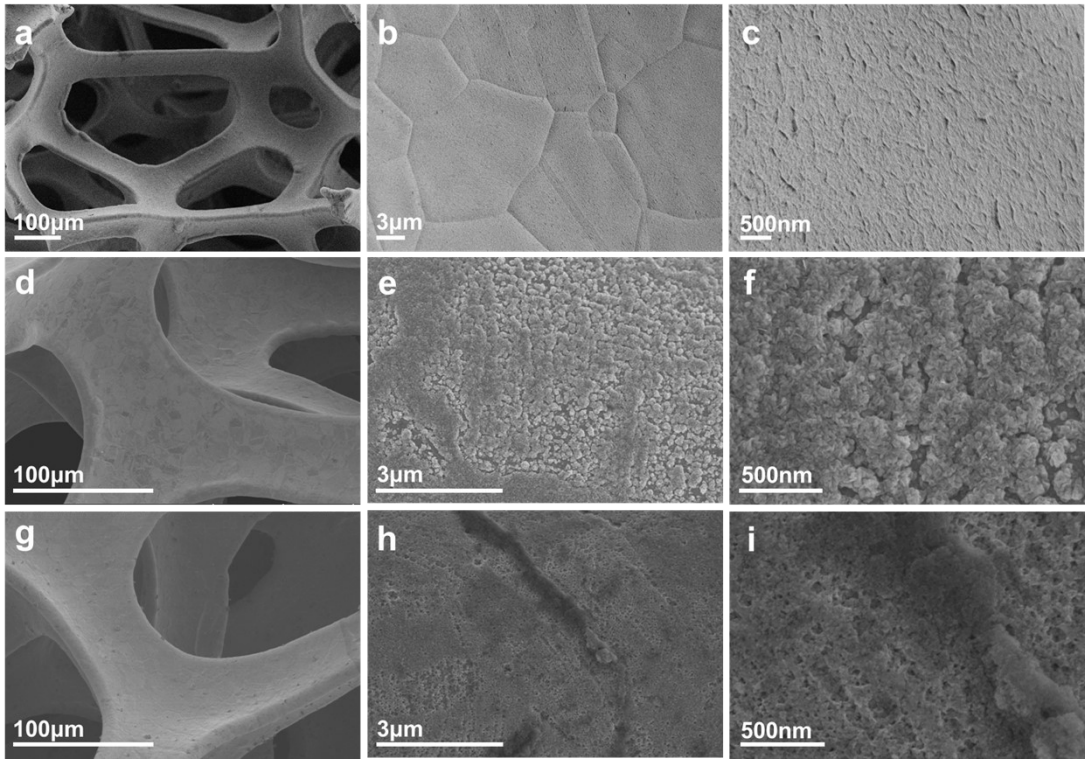

Fig. S3 The SEM images of bare NF (a, b, c), bare NF heated at 450 °C for 3 h with argon protection (d, e, f) and FeCoMnCuOOH before selenization (g, h, i).

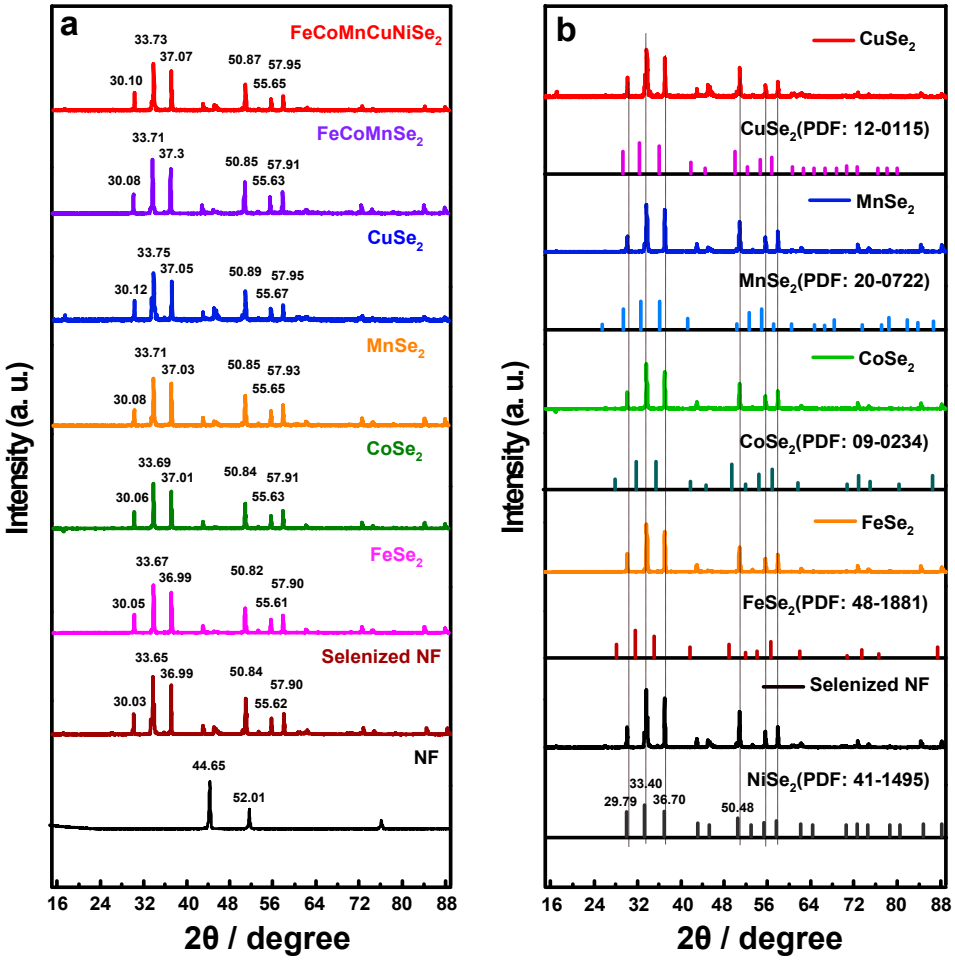

Fig. S4 XRD patterns of $FeCoMnCuNiSe_2$, $FeCoMnSe_2$, $CuNiSe_2$, $FeSe_2$, $CoSe_2$, $MnSe_2$, $CuSe_2$, $NFSe_2$ and NF (a); XRD patterns of $FeSe_2$, $CoSe_2$, $MnSe_2$, $CuSe_2$, selenized NF and JCPDS cards of $CoSe_2$, $FeSe_2$, $CuSe_2$, $MnSe_2$ and $NiSe_2$ (b).

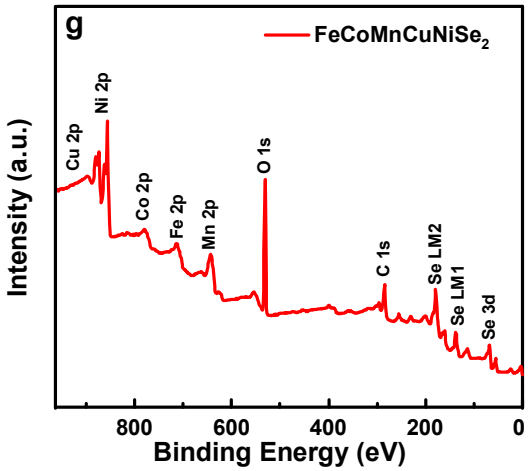

Fig. S5 XPS survey of the $FeCoMnCuNiSe_2$.

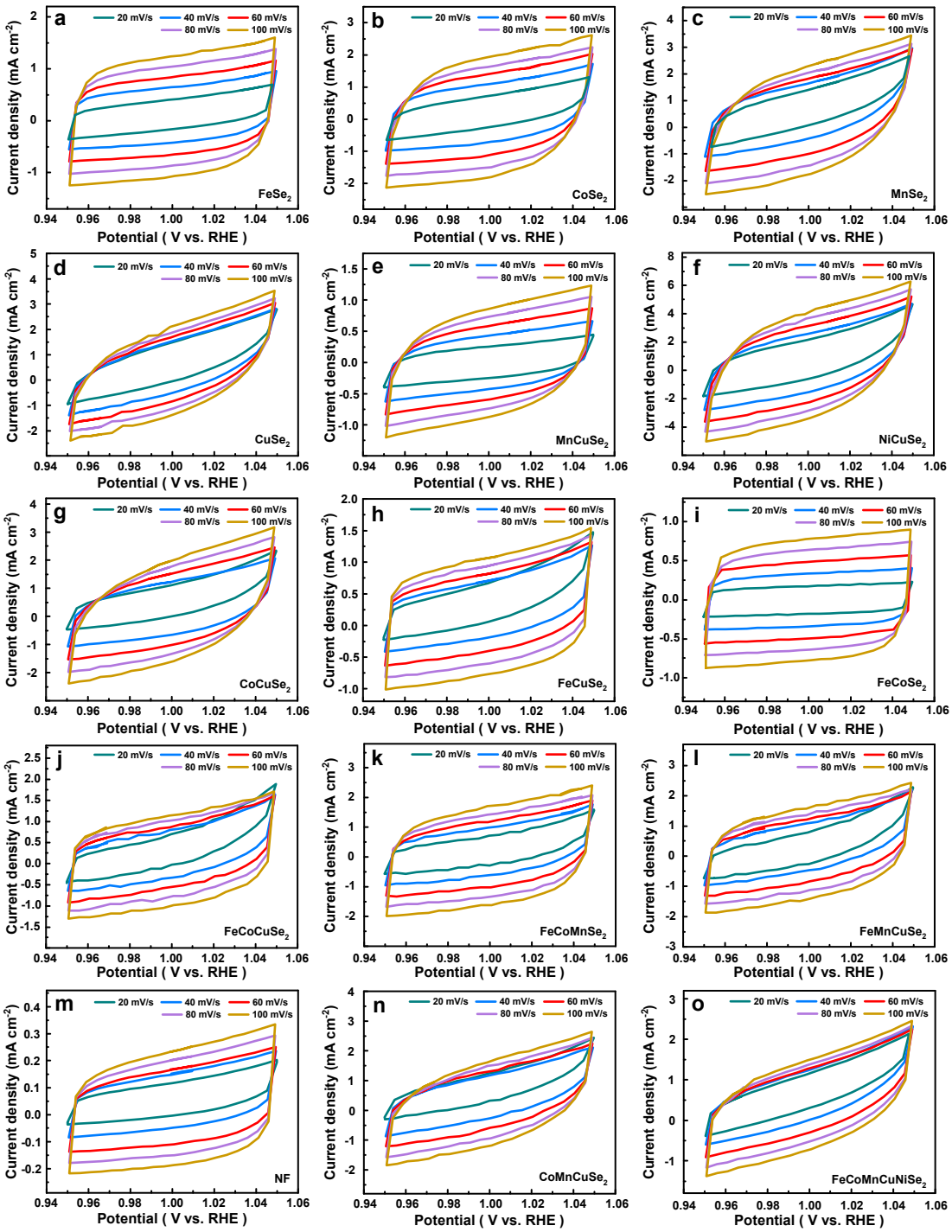

Fig. S6 Cyclic voltammograms for $FeSe_2$ (a), $CoSe_2$ (b), $MnSe_2$ (c), $CuSe_2$ (d), $MnCuSe_2$ (e), $NiCuSe_2$ (f), $CoCuSe_2$ (g), $FeCuSe_2$ (h), $FeCoSe_2$ (i), $FeCoCuSe_2$ (j), $FeCoMnSe_2$ (k), $FeMnCuSe_2$ (l), NF (m), $CoMnCuSe_2$ (n), and $FeCoMnCuNiSe_2$ (o) at the scan rate of 20, 40, 60, 80 and 100 mV s^{-1} in 1.0 M KOH.

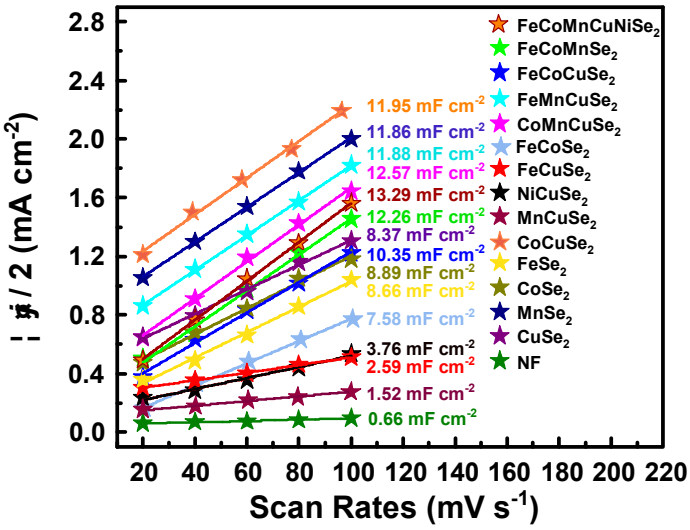

Fig. S7 C_{dl} values of $FeSe_2$, $CoSe_2$, $MnSe_2$, $CuSe_2$, $MnCuSe_2$, $NiCuSe_2$, $CoCuSe_2$, $FeCoCuSe_2$, $FeCuSe_2$, $FeCoSe_2$, $FeCoMnSe_2$, $FeMnCuSe_2$, NF, $CoMnCuSe_2$ and $FeCoMnCuNiSe_2$ at -0.20 V.

In the process of linear scanning, the current displayed by the instrument consists of two parts:

$$i = i_f + i_c \tag{1-1}$$

i_f is faradaic current from electrochemical reaction, i_c is charge and discharge current of the electric double layer, and:

$$i_C = \frac{dq}{dt} = \frac{d(C_{dl}\psi)}{dt} = C_{dl}\frac{d\psi}{dt} + \psi\frac{dC_{dl}}{dt} \tag{1-2}$$

When the potential window in the Faraday region is selected to be smaller, the electric double layer capacitance C_{dl} remains almost unchanged，Then (1-2) can be simplified as:

$$i_C = C_{dl}\frac{d\psi}{dt} \tag{1-3}$$

At the same time, there is a linear relationship between the electrochemical active area and the electric double layer capacitance:

$$ECSA = \frac{C_{dl}}{R} \tag{1-4}$$

where R is a constant in (1-4), C_{dl} is directly used to measure the ECSA of the catalyst.

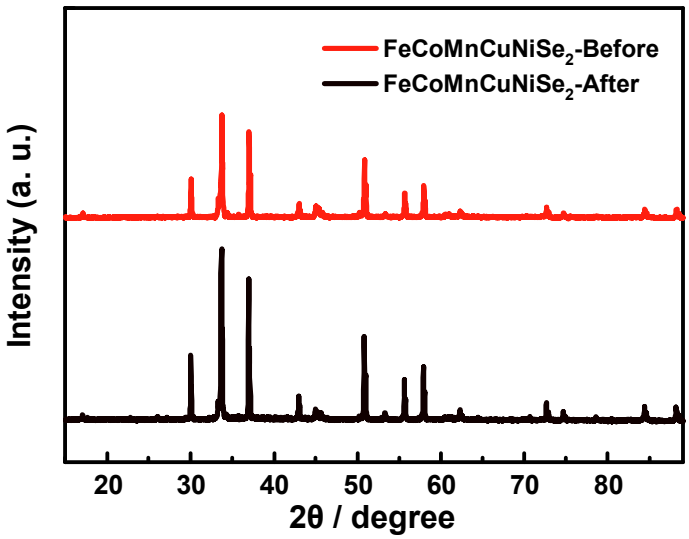

Fig. S8 The XRD spectra of $FeCoMnCuNiSe_2$ before and after 16 h stability.

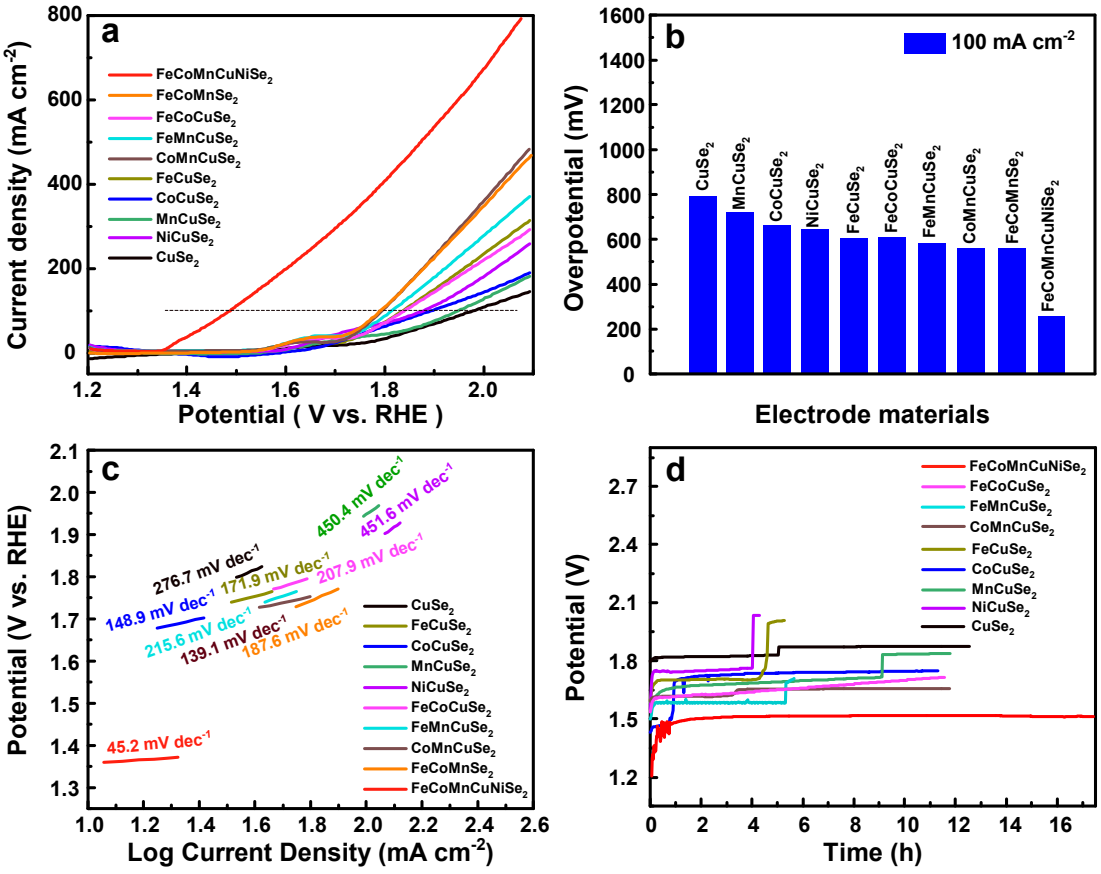

Fig. S9 The OER LSV curves (a), overpotentials at current density of 100 mA cm^{-2} (b), Tafel plots (c), OER durability curves (d) of, $FeCoMnCuNiSe_2$, $FeCoCuSe_2$, $CoMnCuSe_2$, $FeMnCuSe_2$, $FeCuSe_2$, $CoCuSe_2$, $MnCuSe_2$, $NiCuSe_2$ and $CuSe_2$ at 10 mA cm^{-2}.

Table S1 Atomic percentages of Fe, Co, Mn, Cu, Ni in the corresponding solutions of dissolved $FeCoMnCuNiSe_2$ in 6.0 M HCl for 1, 2, 4, 10 min at room temperature and in aqua regia at 170 °C for 36 h.

Time	Fe	Co	Mn	Cu	Ni
1 min	33.0	14.0	24.0	3.0	25.0
2 min	34.0	15.0	28.0	1.0	21.0
4 min	24.0	9.0	15.0	4.0	47.0
10 min	8.0	5.0	10.0	1.0	76.0
36 h	0.54	0.38	0.38	0.34	98.35

Table S2 The HER, OER and OWS performance comparisons of prepared $FeCoMnCuNiSe_2$ to recently reported advanced electrocatalysts.

Catalyst	Support	Overpotential for HER (mV / mA cm^{-2})	Overpotential for OER (mV / mA cm^{-2})	Cell voltage (mA cm^{-2} / V)	Reference
$FeCoMnCuNiSe_2$	**NF**	**71.6/ 100**	**254.8/100**	**100 / 1.51**	This work
0.2-NiSe	NF	95 / 10	-	10 / 1.54	[1]
$NiSe_2$	NF	166 / 10	235/10	10 / 1.64	[2]
$CoO/CoSe_2$	Ti-mesh	337 / 10	-	10 / 2.18	[3]
FeSe	NF	200 / 10	190/100	50 / 1.85	[4]
$CoSe/Co_9Se_8$	NF	268 / 100	280/100	10.3 / 1.8	[5]
CuSe	NF	162 / 10	297/10	10 / 1.68	[6]
$CoNiSe_2$	NF	146 / 100	307/100	10 / 1.59	[7]
$(Ni,Co)Se_2/CoSe_2$	NF	169 / 100	169/100	10 / 1.56	[8]
$(Ni,Co)_{0.85}Se$	NF	169 / 10	287/20	10 / 1.56	[9]
$NiSe_2/Ni_2Se_4$/NF-4	NF	145 / 10	-	10 / 1.56	[10]
$NiSe_2/Ni_2Se_4$/NF-1	NF	185 / 10	337/100		
$NiSe_2$-$NiMoO_4$	NF	-35.6 / -10	-	10 / 1.37	[11]
$Ni_{20}Fe_{20}Mo_{10}Co_{35}Cr_{15}$	-	172 / 10	-	-	[12]
AlNiCoRuMo	-	-24.5 / -10	245/10	-	[13]

CoFeLaNiPt	-	555 / 10	377/10	-	[14]
NiCoFeMnCrP	-	220 / 10	270/10	-	[15]
$FeCoMnNiSe_2$	NF	142.2 / 100	223.1/100	100 / 1.42	[16]

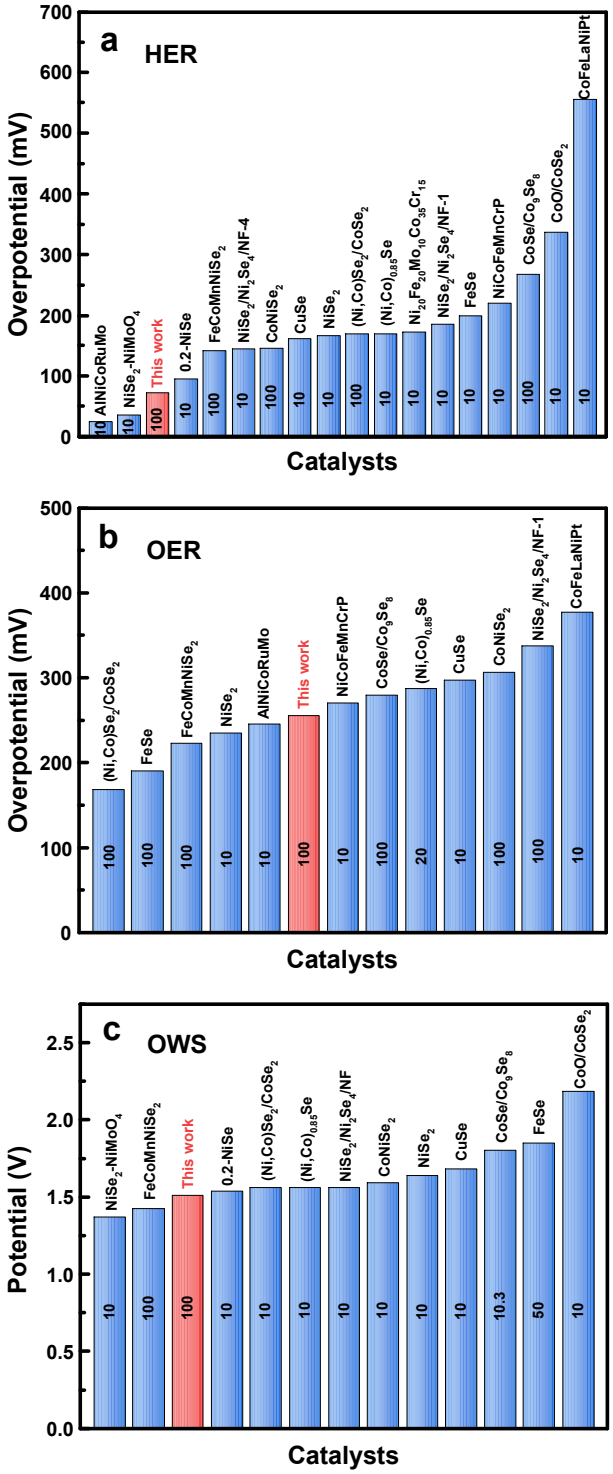

Fig. S10 The HER, OER and OWS performance comparisons of prepared $FeCoMnCuNiSe_2$ to recently reported advanced electrocatalysts.

Video of overall water splitting based on prepared self-standing high-entropy electrode

OWS Video.mp4

References

[1] Y. Li, Y. Zhao, F. M. Li, Z. Y. Dang and P. Q. Gao, Ultrathin NiSe nanosheets on Ni foam for efficient and durable hydrazine-assisted electrolytic hydrogen production, ACS Appl. Mater. Interfaces, 2021, **13**, 34457-34467.

[2] J. Zhang, Y. Wang, C. Zhang, H Gao, L. F. Lv, L. L. Han and Z. H. Zhang, Self- supported porous $NiSe_2$ nanowrinkles as efficient bifunctional electrocatalysts for overall water splitting, ACS Sustain. Chem. Eng., 2018, **6**, 2231-2239.

[3] K. D. Li, J. F. Zhang, R. Wu, Y. F. Yu and B. Zhang, Anchoring CoO domains on $CoSe_2$ nanobelts as bifunctional electrocatalysts for overall water splitting in neutral media, Adv. Mater., 2016, **3**, 1500426.

[4] D. Chanda, R. A. Tufa, Y. Y. Birdja, S. Basu and S. H. Liu, Hydrothermally/electro-chemically decorated FeSe on Ni-foam electrode: An efficient bifunctional electrocatalysts for overall water splitting in an alkaline medium, Int. J. Hydrog. Energy, 2020, **45**, 27182-27192.

[5] Y. Q. Zhao, B. Jin, Y. Zheng, H. Y. Jin, Y. Jiao and S. Z. Qiao, Charge state manipulation of cobalt selenide catalyst for overall seawater electrolysis, Adv. Energy Mater., 2018, **8**, 1801926.

[6] B. Chakraborty, R. Beltrán-Suito, V. Hlukhyy, J. Schmidt, P. W. Menezes and M. Driess,

Crystalline copper selenide as a reliable non-noble electro(pre)catalyst for overall water splitting, ChemSusChem, 2020, **13**, 3222-3229.

[7] T. Chen and Y. Tan, Hierarchical $CoNiSe_2$ nano-architecture as a high-performance electro-catalyst for water splitting, Nano Res., 2018, **11**, 1331-1344.

[8] J. J. Zhu, Y. K. Lu, X. Y. Zheng, S. J. Xu, S. C. Sun, Y. Liu, D. Li and D. L. Jiang, Heterostructure arrays of $(Ni,Co)Se_2$ nanowires integrated with MOFs-derived $CoSe_2$ dodecahedra for synergistically high-efficiency and stable overall water splitting, Appl. Surf. Sci., 2022, **592**, 153352.

[9] K. M. Xiao, L. Zhou, M. F. Shao and M. Wei. Fabrication of $(Ni, Co)_{0.85}Se$ nanosheet arrays derived from layered double hydroxides toward largely enhanced overall water splitting, J. Mater. Chem. A, 2018, **6**, 7585-7591.

[10] L. Tan, J. T. Yu J, H. Y. Wang, H. T. Gao, X. Liu, L. Wang, X. L. She and T. R. Zhan, Controllable synthesis and phase-dependent catalytic performance of dual-phase nickel selenides on Ni foam for overall water splitting, Appl. Catal. B, 2022, **303**, 120915.

[11] T. Q. Yu, Q. L. Xu, J. L. Chen, G. F. Qian, X. Y. Zhou, H. F. Yang and S. B. Yin, Boosting urea-assisted water splitting by constructing sphere-flower-like $NiSe_2$-$NiMoO_4$ heterostructure, Chem. Eng. J., 2022, **449**, 137791.

[12] G. L. Zhang, K. S. Ming, J. L. Kang, Q. Huang, Z. J. Zhang, X. R. Zheng and X. F. Bi, High entropy alloy as a highly active and stable electrocatalyst for hydrogen evolution reaction, Electrochim. Acta, 2018, **279**, 19-23.

[13] Z. Y. Jin, J. Lyu, Y. L. Zhao, H. L. Li, X. Lin, G. Q. Xie, X. J. Liu, J. J. Kai and H. J. Qiu, Rugged high-entropy alloy nanowires with in situ formed surface spinel oxide as highly

stable electrocatalyst in Zn-air batteries, ACS Mater. Lett., 2020, **2**, 1698-1706.

[14] M. W. Glasscott, A. D. Pendergast, S. Goines, A. R. Bishop, A. T. Hoang, C. Renault and J. E. Dick, Electrosynthesis of high-entropy metallic glass nanoparticles for designer, multi-functional electrocatalysis, Nat. Commun., 2019, **10**, 2650.

[15] D. W. Lai, Q. L. Kang, F. Gao and Q. Y. Lu, High-entropy effect of a metal phosphide on enhanced overall water splitting performance, J. Mater. Chem. A, 2021, **9**, 17913-17922.

[16] Z. W. Liu, X. X. Guo, T. L. Cui, S. H. Mu, Z. H. Ni, C. Z. Zhang and S. J. Lu. Porous freestanding $FeCoMnNiSe_2$ medium-entropy bifunctional electrocatalyst for oxygen and hydrogen evolution reactions in alkaline medium, J. Power Sources, 2024, **592**, 233956.